PROCEEDINGS A

royalsocietypublishing.org/journal/rspa

Research

Cite this article: Ramananarivo S, Mitchel T, Ristroph L. 2019 Improving the propulsion speed of a heaving wing through artificial evolution of shape. *Proc. R. Soc. A* **475**: 20180375.
http://dx.doi.org/10.1098/rspa.2018.0375

Received: 5 June 2018
Accepted: 3 January 2019

Subject Areas:
fluid mechanics, biomechanics, mechanical engineering

Keywords:
flapping flight, flow–structure interaction, optimal locomotion, evolutionary algorithm, undulatory swimming

Author for correspondence:
Sophie Ramananarivo
e-mail: sophie.ramananarivo@gmail.com

Improving the propulsion speed of a heaving wing through artificial evolution of shape

Sophie Ramananarivo†, Thomas Mitchel and Leif Ristroph

Applied Math Lab, Courant Institute, New York University, New York, NY 10012, USA

SR, 0000-0003-1049-4131

Aeronautical studies have shown that subtle changes in aerofoil shape substantially alter aerodynamic forces during fixed-wing flight. The link between shape and performance for flapping locomotion involves distinct mechanisms associated with the complex flows and unsteady motions of an air- or hydro-foil. Here, we use an evolutionary scheme to modify the cross-sectional shape and iteratively improve the speed of three-dimensional printed heaving foils in forward flight. In this algorithmic-experimental method, 'genes' are mathematical parameters that define the shape, 'breeding' is the combination of genes from parent wings to form a daughter, and a wing's measured speed is its 'fitness' that dictates its likelihood of breeding. Repeated over many generations, this process automatically discovers a fastest foil whose cross-section resembles a slender teardrop. We conduct an analysis that uses the larger population to identify what features of this shape are most critical, implicating slenderness, location of maximum thickness and fore-aft asymmetries in edge sharpness or bluntness. This analysis also reveals a tendency towards extremely thin and cusp-like trailing edges. These findings demonstrate artificial evolution in laboratory experiments as a successful strategy for tailoring shape to improve propulsive performance. Such a method could be used in related optimization problems, such as tuning kinematics or flexibility for flapping propulsion, and for flow–structure interactions more generally.

†Present address: LadHyX, UMR 7646 du CNRS, École polytechnique, 91128 Palaiseau Cedex, France.

Electronic supplementary material is available online at https://dx.doi.org/10.6084/m9.figshare.c.4369949.

THE ROYAL SOCIETY PUBLISHING

1. Introduction

The adage 'shape matters' aptly applies to aerodynamics and aeronautics. Many of the innovations and improvements in fixed-wing aviation, as well as in propulsion through and on water, have involved better understanding how the shapes of structures affect the flows and forces generated [1,2]. Flapping-wing flight and undulatory swimming involve distinct fluid-dynamical effects such as separated flows, vortex formation and other unsteady phenomena. Rather than operating under conditions of smooth and attached flow, these locomotion modes are characterized by the repeated generation and shedding of vortices due to oscillations of a wing or fin [3]. One thus expects distinct, and perhaps all the more nuanced, ways in which the shape of an air- or hydro-foil is linked to its propulsive performance. Better understanding these mechanisms could shed light on the different strategies employed by swimming and flying animals and could also be applied to the design of biomimetic or biologically inspired robots. These different incentives have driven a renewed scientific and engineering interest in flapping propulsion [4,5], which has served as an archetypal problem in fluid–structure interactions in recent decades.

Pioneering studies first showed that heaving or pitching motions of a foil produce forward thrust [6–9], and subsequent efforts have sought to identify the relevant mechanisms by examining the force distribution over the surface and the unsteady flows generated. A notable effect is that of leading-edge suction, in which the motion at angle of attack leads to a low-pressure region that is associated with fast flow around the front of the foil [9–11]. Another prominent feature is the reverse von Kármán wake in which an array of staggered and counter-rotating vortices yield a backwards jet-like flow downstream of the foil [12–16]. The momentum in the wake is a signature of thrust production, and the strength of the jet is related to the arrangement and intensity of vortices. Recent studies have focused on how vortices form and shed by boundary layer separation as well their subsequent dynamics and interactions with one another and with the foil surface [14,17–23].

The variety and complexity of effects suggest many avenues by which flapping propulsion might be controlled and optimized, and previous studies have focused primarily on wing kinematics and flexibility. Conditions of high performance have been attained for combined heaving and pitching motions [17,24–26], and the forward speed of a wing has been optimized with respect to the stroke waveform during up-and-down heaving [27]. Studies have also shown that, for fixed motions and shape, there exists an optimal degree of wing flexibility for both propulsive speed and efficiency [28–31]. Less studied is the role played by foil shape. Previous studies have investigated a restricted family of foils in order to focus on specific features in isolation, such as thickness distribution [32–38], camber [32,37,39] and edge geometry [40]. Furthermore, studies employing different simulation or modelling methods have led to seemingly contradictory conclusions, for example, with regard to optimal aerofoil thickness [37,41]. Overall, experiments that explore a broad array of foil profiles could offer a more complete picture of the role of shape in flapping locomotion.

A current challenge is to perform a more global search of the vast shape-space. Evolutionary or genetic algorithms are well suited for such optimizations that involve many parameters and potentially complex landscapes for how a specified objective depends on these parameters [42–44]. In recent decades, this approach has been increasingly applied to a variety of engineering problems [45,46] and specifically to optimize hydrodynamic properties of structures propelling in a fluid [47–50]. While these algorithms cannot guarantee true optimality of the best-found solution, such a claim can often in practice be corroborated through additional investigations. Evolutionary algorithms are also useful as a means to explore a landscape while improving a specified objective, and for this reason, they have also emerged as a valuable tool to gain insight into underlying physical mechanisms [51,52]. And while such algorithms perform better for large population sizes and many generations, past studies have been successful with relatively small samples [47,53].

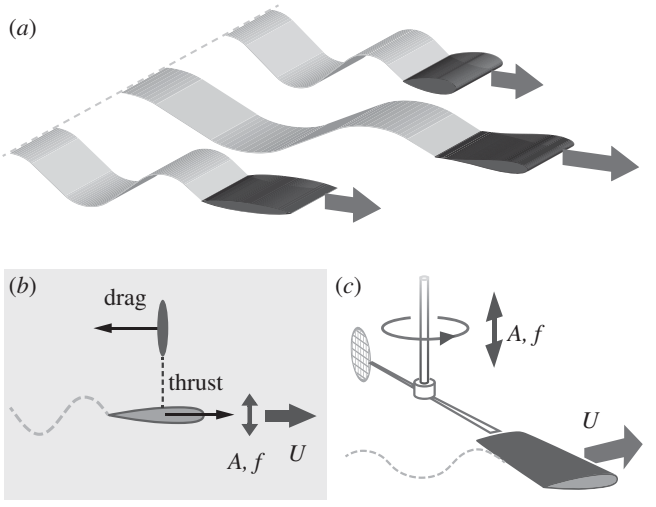

Figure 1. Effect of shape on the forward flight of a heaving and plunging wing. (*a*) A race among wings or foils of varying cross-section. (*b*) Problem idealization: A wing is driven to heave up and down with amplitude A and frequency f, resulting in self-propulsion through a fluid while towing a drag payload. The steady-state speed U is set by the balance of thrust and drag, which depends on the shape. (*c*) Experimental realization: A three-dimensional printed foil is connected to an upright shaft through which a vertical heaving motion is imposed, and rotary bearings allow for forward propulsion in orbits around a water tank.

Here, we combine an evolutionary algorithm with laboratory experiments to explore the role of propulsor shape in controlling and optimizing flapping locomotion. Specifically, we seek ideal wing profiles for fast locomotion through an evolutionary or genetic scheme that permits an extensive search of shapes whose performance can be efficiently and directly measured. To isolate the effect of profile shape alone, we consider the simplified case of a heaving, rigid foil of uniform spanwise shape but whose cross section can be varied and realized by three-dimensional printing. These foils self-propel through water, and the fastest individuals are preferentially selected in forming a new generation of wings that inherit favourable shape traits. By repeating this process, many cross-sectional shapes are explored as speed is iteratively improved. The central aim of this work is to identify the shape features favourable for fast propulsion and, in particular, to test whether an evolutionary algorithm can automatically 'discover' such ideal foil profiles. If so, such a method may be applied to improving or optimizing other aspects of flapping locomotion, such as more complex kinematics, flexibility and spanwise shape variations. Indeed, such an approach could prove useful in fluid–structure interaction problems generally.

2. Algorithmic-experimental approach

This work focuses on the following question: Given a particular heaving motion, and given a fixed amount of material (i.e. cross-sectional area) from which to make a wing or hydrofoil, what profile shape yields the fastest locomotion? Which wing emerges as the winner of a race among different shapes, as illustrated in figure 1*a*? The fluid dynamical situation being considered is shown in figure 1*b*: A rigid wing or hydrofoil undergoes prescribed up-and-down motion of peak-to-peak amplitude A and frequency f within a fluid. Forward flight or self-propulsion at a terminal speed U is attained once the thrust produced by the foil comes into balance with the resistance incurred by a drag payload that is towed along. This idealized scenario might be viewed as analogous to forward flapping flight or swimming, where wings or fins generate thrust to overcome the drag on a body.

Our experimental realization involves an apparatus for 'test-flying' three-dimensional printed foils through water and measuring the speed. As schematized in figure 1*c*, a foil is affixed to one end of a horizontal rod, which itself is attached to an upright shaft (see also electronic supplementary material, Movie S1). The shaft is driven to heave sinusoidally up and down by a motor (not shown) at prescribed A and f, and this flapping motion is imparted to the foil. The motor connects to the shaft via low-friction rotary bearings, which allow for free rotation of the foil about the upright shaft. Swimming or flying thus takes the form of orbits around a cylindrical water tank, and such a rotational system has been shown in previous studies to share important features with translational locomotion [13,14,33]. When driven to heave, the wing 'takes off' from rest and soon attains a terminal rotational speed, which is automatically recorded by an optical encoder and converted to a translational speed U at the mid-span. We implement a drag payload in the form of a grid damper that is affixed opposite to the foil on the horizontal rod. By slowing the swimming with the damper, along with implementing a long circumferential travel distance around the tank, we ensure that the flows generated in the previous orbit are largely dissipated and have minimal influence (see Material and Methods). Our approach exploits three-dimensional printing to manufacture rigid wings of a wide variety of cross-sectional forms, each of which can be readily attached to the device in order to measure speed for different kinematics.

To focus on the role of cross-sectional shape in thrust generation, we impose a number of simplifications and idealizations. The wings are rigid, and the shapes are uniform in the span-wise direction to yield a quasi-two-dimensional situation. We consider sinusoidal heaving-and-plunging rather than more complex flapping kinematics involving pitching rotations. This case of heaving flight of a rigid wing, while idealized in comparison to natural flight, has served as an archetypal flapping flight problem in past studies and retains many of the relevant fluid dynamical complexities [19,33–37]. We consider a fixed peak-to-peak flapping amplitude $A = 3$ cm and vary flapping frequency $f = 0.4$–2.4 Hz, though we find that the relative ranking in terms of speed of different foils does not differ significantly for different values of f. That is, speed U typically increases with f for all wings, but if wing A is faster than wing B for $f = 1$ Hz, then A tends to be faster than B at $f = 2$ Hz as well (see Material and Methods). We also seek to optimize locomotion speed, as opposed to other objectives such as efficiency, in order to reveal mechanisms for thrust production. We demand that all foils share the same cross-sectional area and the same span length, or equivalently, the same total volume. This leads to shapes of differing chord length c, and because we consider fixed heaving amplitude A, the dimensionless amplitude A/c is not uniform across foils. After the presentation of our findings for this case study, we speculate as to how the optimal shape may change for other conditions and other objectives, all extensions for which the methods presented here may be applied.

As shown in figure 2*a*, we explore wing shapes that are up-down symmetric but may have the fore-aft asymmetries that likely play a role in thrust production. The profile is specified by a function $y(x)$ for the upper surface, and different shapes are attained by different values for input parameters. Specifically, we introduce a modified version of classic NACA aerofoils in which $y(x)$ takes the form of a polynomial with a square-root term that allows for blunt edges. The equation is provided in the Material and Methods section below, and each wing is uniquely identified by a set of coefficients in this formula. These parameters can be viewed as 'genes' that can be grouped into a genome vector $\boldsymbol{g}$ for each individual. Importantly, our formula admits a rich variety of shapes, with some examples shown in figure 2*b*. Variations include fore-aft symmetric shapes that resemble an ellipse or lens, or asymmetric shapes such as a classic aerofoil. The leading and trailing edges can be blunt and rounded or sharp and angular.

The genes defining a wing's shape, as well as the measured speed that serves as its 'fitness', provide the inputs to a genetic or evolutionary algorithm that seeks to improve the speed by modifying shape. We employ an established evolutionary scheme [54] selected from a class of algorithms that has proven successful even for cases in which the population size within a generation and the number of generations are limited [47,55]. Starting with an initial population of ten shapes, our scheme iteratively produces new generations by preferentially cross-breeding faster wings, as shown in figure 2*c* and further detailed in the Material and Methods section.

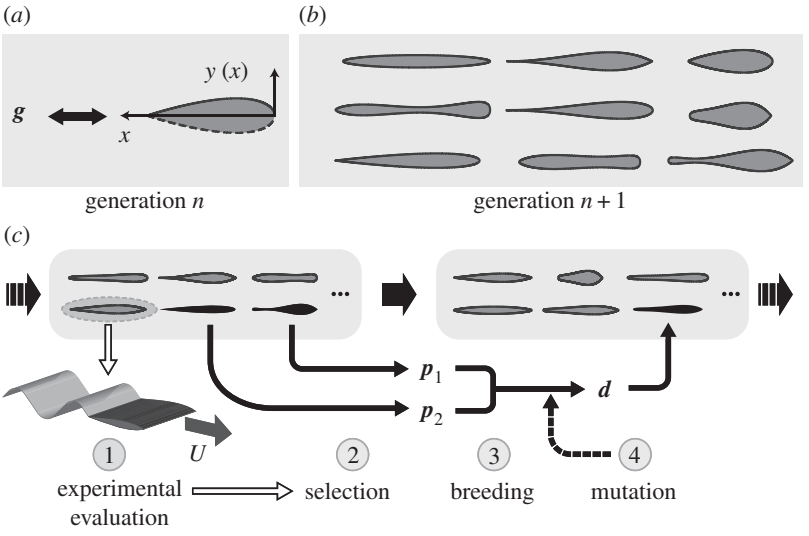

Figure 2. Artificial evolution of wing cross-sectional shape. (*a*) The upper surface of an up-down symmetric foil, $y(x)$, is given by a functional form with a set of input parameters $\boldsymbol{g}$ representing 'genes' specific to each individual. (*b*) This shape parametrization admits many forms. (*c*) Algorithmic-experimental evolution scheme: Parent wings are selected from one generation with a probability based on their experimentally measured speed U. These wings then breed by combining and mutating genes to form a daughter wing who becomes a member of the next generation.

For each generation, the speed U of all individuals is first measured across the tested flapping frequency range, and a fitness parameter is evaluated that factors in performance for all f. This frequency-averaged fitness is a robust characterization of the relative performance or speed-ranking for all wings in the generation. To begin populating the next generation, two individuals are selected for 'breeding', with the selection probability specified to be an increasing function of speed. Breeding involves a mathematical operation that combines the genomes $\boldsymbol{p_1}$ and $\boldsymbol{p_2}$ of two parents to form a daughter wing $\boldsymbol{d}$ that tends to resemble its parents. We also impose mutations that randomly perturb gene values, potentially generating new traits and thus promoting variability within the population. This process is repeated to form eight wings in the next generation, whose population of ten is completed by carrying over the two fastest shapes unmodified. Iteration over many generations is expected to improve the speed.

3. Evolutionary trends and the fastest shape

To carry out the evolution scheme, we seed the first generation with slender shapes expected to perform well but also with a variety of characteristics. These initial members include forms such as a NACA aerofoil, a shape resembling an ellipse and geometries with varying degrees of bluntness and sharpness at both edges. We then implement the scheme described above. Figure 3*a* shows the normalized speed U/Af for the 10 members of each generation over 15 such iterations, with each dot corresponding to a single individual. For clarity, we present data in this and subsequent plots for an intermediate frequency $f = 1.8$ Hz, which is representative of trends across all $f \in [0.4, 2.4]$ Hz. The performance of the fastest member of each generation can be seen to improve markedly in under 10 generations. The top speed within each generation increases by 20% and then reaches a plateau, suggesting that the algorithm has progressed towards an optimum. The fastest wing among all shapes first appears at the 11th generation and then remains in all subsequent generations. It is denoted by red stars on the graph, and its shape is shown in red in figure 3*a*. A significant spread in the speeds within each generation persists throughout the process, which indicates high variability in the population. The variability is kept high due

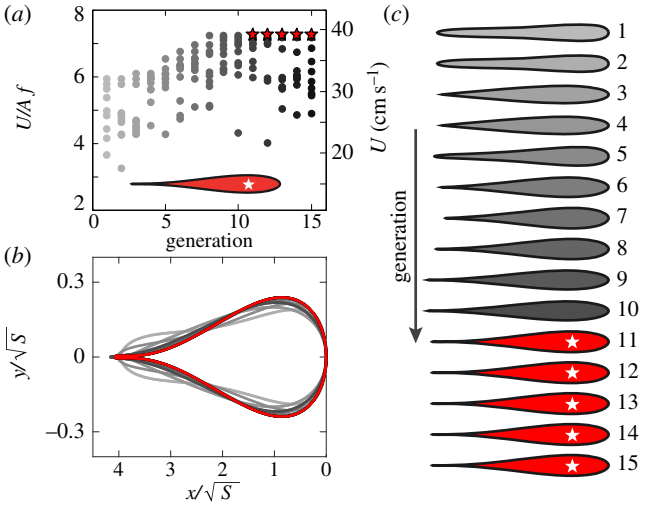

Figure 3. Emergence of a fastest wing shape. (*a*) Normalized speed U/Af increases over successive generations and then reaches a plateau. Dots represent the 10 wings in each generation, and the fastest solution (star) is produced in the 11th generation. Data are shown for $f = 1.8$ Hz. (*b*,*c*) The fastest wing of each generation: (*b*) Superposition of normalized profiles, where S is the cross-sectional area. The foil shapes are compressed horizontally to better display the development over generations. (*c*) The fastest foils from each generation shown at proper relative scale.

to the substantial level of mutation in the genetic algorithm, which promotes exploration of the high-dimensional shape space (see Material and Methods). While the scheme is not guaranteed to produce a true optimum, it does seem to have yielded a unique fastest individual after this broad search.

The propulsive speeds attained determine the fluid dynamical regime in which the foils operate, which is characterized by the Reynolds and Strouhal numbers and the reduced frequency. Our data yield Reynolds numbers within $Re = Uc/\nu \backsim 10^3 - 10^4$, where U is the swimming speed, c is the wing chord length and ν is the kinematic viscosity of water. The observed range of Re partially overlaps with those for bird flight and fish swimming. The Strouhal number $St = Af/U$ is an important determinant of vortex shedding for heaving foils, and here $St = 0.14 - 0.31$, which also overlaps with that of animals [56]. In figure 3*a*, we display the inverse of the Strouhal number, U/Af as a measure of the output swimming speed U for a characteristic input heaving speed Af. This regime of Re and St is marked by flow separation and the roll-up of vortices at the leading and trailing edges subsequently impacting the thrust generated [19]. The reduced frequency $k = fc/U$ is a measure of unsteadiness and may be viewed as a ratio of time-scales: c/U is the typical time a fluid parcel may interact with the passing foil, and $1/f$ is the flapping period. The present study explores $k = 0.3 - 0.6$. The three parameters Re, St and k are typically imposed in fixed-velocity studies but are outcomes here, as c is an evolved quantity and U is the resulting speed for a given shape.

The progression towards the fastest shape also provides a number of interesting insights. In the first generation, for example, the classic NACA aerofoil unexpectedly loses to the wing shown at the top of figure 3*c* which has rounded leading and trailing edges. Furthermore, one can examine the progression of the fastest shape within each generation, and these profiles are shown in figure 3*b*,*c*, where shades of grey denote generational progression and the global fastest form is shown in red. Figure 3*b* shows these elite profiles overlaid and re-scaled to highlight the subtle differences, and it can be seen that much of the initial development occurs at the trailing edge. Later forms appear to converge to the fastest shape, again suggesting approach to an optimum. Figure 3*c* shows these same forms at proper scale.

Slenderness is the most salient feature shared by the elite, and the most apparent overall developments are the formation of fore-aft asymmetries and a sharp trailing edge. Close inspection of all these data shows that the modest improvement in generations 1–4 is associated with the formation of an angular trailing edge, while the more marked progression from 4 to 8 seems linked to its evolution into a thin cusp. In fact, we found that in later generations the algorithm occasionally produced shapes so thin that we were unable to three-dimensional print them successfully. (This occurred once in generation 11 and twice in generation 12.) In such cases, the unprintable shape was simply replaced with a new printable daughter wing generated by again selecting and breeding two parents in the previous generation. These events seem to be examples of the optimization procedure leading to shape solutions that are unphysical (e.g. infinitesimally thin) and thus unrealizable due to practical manufacturing limitations.

This study has generated a wealth of data on the locomotion speed of 150 wing forms heaved at 11 different frequencies, for a total of 1650 measurements, all of which are available as electronic supplementary material.

4. Eigenmorphs: a genomic basis linked to fitness

We next pursue a more systematic means to identify the aspects of shape most crucial for speedy propulsion. Our procedure takes advantage of the large database on foils of differing shapes and employs a statistical analysis to relate genetic variations to performance. Our method employs principal component analysis (PCA) and can be motivated by a simple, illustrative example involving only two genes, g_1 and g_2. In figure 4*a*, we show schematically how a population of the fastest foils (each represented by a circle) may be distributed in this two-dimensional gene space about the optimal solution (star). Generically, there will be directions of differing variability, and the new directions $\boldsymbol{e_1}$ and $\boldsymbol{e_2}$ represent small and large variations, respectively. PCA identifies these as eigenvectors (or principal components) of increasing eigenvalue, and these new directions can be expressed as linear combinations of the original directions. Importantly, the variations across individuals are uncorrelated for these new genes whereas they are correlated in the original genes. We suggest that the new directions form a more natural genomic basis for parametrizing shape as it is relevant to performance. For example, the new gene $\boldsymbol{e_1}$ represents a change of shape that is sparsely represented among the elite foils, and thus we infer that this morphing is highly detrimental to performance. This new gene may be called 'stiff' as it seems tightly constrained (as if by a stiff spring) and ought not be varied much if performance is to be maintained. The new gene $\boldsymbol{e_2}$ is a 'soft' direction that is weakly constrained (as if by a soft spring), and large variations do not degrade performance significantly.

We implement this procedure to identify the eight new genes or directions in the genome space for the eight-component shape parametrization outlined in the Material and Methods. The fastest 40 wings are selected and we use PCA to identify these new directions as those along which the variations across individuals are uncorrelated. The analysis centres the gene pool around the mean genome $\boldsymbol{m}$, which is near the optimum, and applies a singular value decomposition to the resulting data matrix. Each of the eight newly identified variables dictates a specific morphing of foil shape. Hence, we use the term 'eigenmorph' for each new gene or direction in genomic space. Table 1 reports on the eigenmorphs as revealed by PCA, where the new shape space directions are expressed in terms of the original gene parameters.

In figure 5*a*, we show how wing shape is distorted from the mean shape $\boldsymbol{m}$ by incrementally scanning along each eigenmorph $\boldsymbol{e_i}$ separately. That is, the shapes shown correspond to $\boldsymbol{m} + \mu \boldsymbol{e_i}$, where μ is a parameter that is varied to 'walk' along each eigenmorph. Note that sufficiently large $|\mu|$ along any $\boldsymbol{e_i}$ leads to shapes outside the elite family. As in the simple 2-gene example given above, the eigenmorphs have differing degrees of variability that may be interpreted in terms of how changes in shape impact performance. The eight eigenmorphs of figure 5*a* are ordered and numbered by increasing variance, measured by their respective eigenvalues λ_i. The variance along each direction is shown in figure 5*b*, where we have normalized such that their

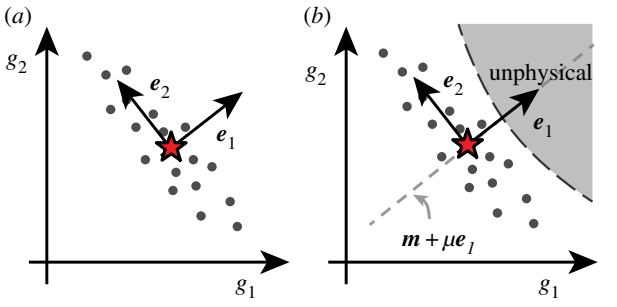

Figure 4. Schematic illustrating the eigenmorph analysis. (*a*) For a two-gene system, the fittest or most elite individuals (grey dots) will exhibit variability about the optimum $\boldsymbol{m}$ in the gene space (g_1, g_2). The eigenmorphs ($\boldsymbol{e_1}$, $\boldsymbol{e_2}$) are a new basis with uncorrelated variations. The under-representation of fit individuals along the 'stiff' direction $\boldsymbol{e_1}$ suggests that the associated shape changes are detrimental. The 'soft' eigenmorph $\boldsymbol{e_2}$ is associated with less detrimental shape changes. (*b*) Stiff and soft directions naturally arise when the optimal solution is near the boundary of an inaccessible region in the gene space. (Online version in colour.)

Table 1. Mean genome $\boldsymbol{m}$ of the population of 40 fastest wings, and new gene parametrization $\{e_i\}$ derived from PCA and expressed in the original genomic basis $\{g_i\}$.

	g_1	g_2	g_3	g_4	g_5	g_6	g_7	g_8
$\boldsymbol{m}$	0.208	−0.185	−0.144	0.210	0.906	0.905	0.974	0.484
$\boldsymbol{e_1}$	−0.266	0.117	0.956	0.000	0.012	−0.023	0.015	−0.002
$\boldsymbol{e_2}$	0.874	0.432	0.192	−0.086	0.008	0.021	−0.0604	0.0211
$\boldsymbol{e_3}$	0.256	−0.613	0.163	0.021	−0.006	0.727	0.066	0.005
$\boldsymbol{e_4}$	−0.005	0.243	−0.031	0.898	−0.082	0.159	0.314	−0.056
$\boldsymbol{e_5}$	0.196	−0.340	0.070	0.056	0.645	−0.413	0.500	0.040
$\boldsymbol{e_6}$	−0.072	0.111	−0.029	0.177	0.659	0.182	−0.583	−0.378
$\boldsymbol{e_7}$	0.137	−0.328	0.081	0.364	−0.075	−0.310	−0.535	0.589
$\boldsymbol{e_8}$	−0.192	0.360	−0.094	−0.137	0.370	0.383	0.132	0.711

sum is unity: $\sigma_i = \lambda_i / \sum_j \lambda_j$. The inverse of this normalized variance, which we associate with stiffness, is plotted on logarithm-scale in figure 5*c*. The first eigenmorph has the least variance, it is the stiffest, and the associated changes in the genes along this direction are most sparsely represented in the elite gene pool. We interpret this under-representation among the fastest foils as indicating that the associated changes in shape are highly detrimental to performance. From figure 5*c*, one sees that eigenmorphs 1 and 2 are particularly important, with a stiffness that is about an order of magnitude greater than that of eigenmorph 3. In the section that follows, we interpret these stiffest eigenmorphs in terms of what aspects of shape are most critical for fast propulsion.

The softer eigenmorphs have greater variance, and the associated variations in genes along these directions are well represented among the elite. Such a soft direction could be understood to indicate that the associated changes to shape are only weakly detrimental to performance. It could also be that the changes in gene parameters corresponding to a soft eigenmorph do not actually lead to much change in shape, as seems to be the case for eigenmorph 6, for example. In this case, the soft eigenmorph could be viewed as indicating over-parametrization or redundancy of genes, at least for those genomes in the vicinity of the optimal solution.

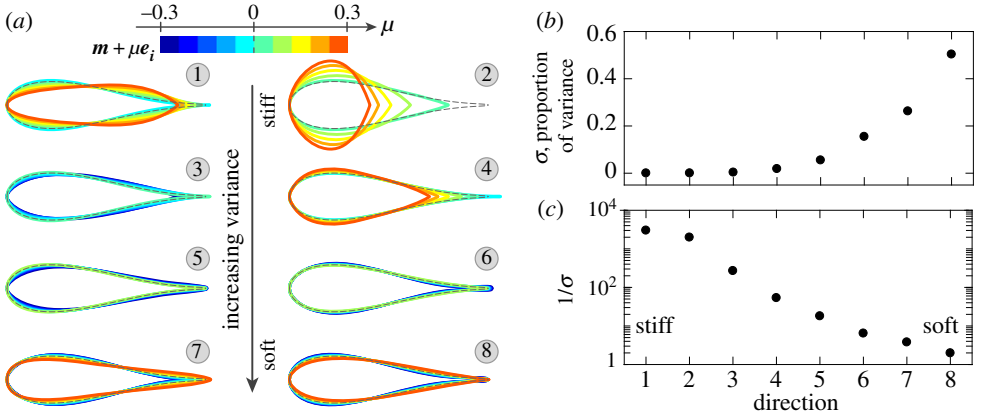

Figure 5. Eigenmorphs constructed from analysis of the 40 fastest foils. (*a*) Eight eigenmorphs as identified by PCA and ordered from stiff or low variance to soft or high variance. For each, we display the shapes that arise when the optimal foil $\boldsymbol{m}$ (dashed outline) is perturbed along the associated direction $\boldsymbol{e_i}$ in shape space: $\boldsymbol{m} + \mu\, \boldsymbol{e_i}$ with $\mu \in [-0.3, 0.3]$ exploring about three times the maximal spread in this elite population. The wing thickness is scaled by a factor of two for all foils to highlight changes. (*b*) Proportion of the total variance σ accounted by each eigenmorph. (*c*) Inverse of σ as a measure of the stiffness of each eigenmorph.

5. Identifying favourable shape characteristics

The above analysis suggests that the most crucial aspects of shape for ensuring speedy propulsion can be gleaned from the stiffest eigenmorphs. Examination of the associated changes in shape from figure 5*a* indicates several important features. The most prominent feature that is changed in eigenmorph 1 is fore-aft asymmetry. The rounded front region and slender back region of the optimal solution (dashed curve) is destroyed and the asymmetry in thickness distribution is even inverted for $\mu > 0$ to give a slimmer nose than tail. Sharpness of the edges is one aspect of this asymmetry, along with the location of maximum chord thickness. The optimal wing is thickest near the front, and scanning along the first eigenmorph causes this location to move backward on the wing. The most prominent feature of the second eigenmorph is the chord length or, equivalently, the slenderness of the foil, as may be quantified by the thickness-to-chord aspect ratio. In addition to the loss of slenderness, one again sees a general loss of fore-aft asymmetry as the edges become more similar in sharpness and the position of maximum thickness approaches the mid-chord.

Related to the fore-aft asymmetry in edge sharpness, the exceedingly thin trailing edge of the optimal foil is seen to be destroyed for $\mu > 0$ in both eigenmorphs 1 and 2. Less apparent from figure 5*a* is what happens for $\mu < 0$, in which case we find that the foil is morphed into an unphysical shape (not displayed) as the foil profile curve crosses itself near the trailing edge. (That is, the thickness curve $y(x)$ for the upper profile takes on negative values.) In essence, it seems the optimal foil is so tapered at the trailing edge that even small changes in shape cause the upper and lower profile curves to intersect. We suggest that the situation may be akin to that shown schematically in figure 4*b*: the optimal solution is near an unphysical boundary, leading to stiff eigenmorphs that are normal to this boundary. To explore this idea, we introduce a metric for trailing-edge fineness τ, defined as the cross-sectional area of the wing divided by the area of the portion over the last fourth along the chord. For example, a wing with uniform thickness (i.e. rectangular cross-section) would be given a low value of $\tau = 4$, while a high value of $\tau = 100$ corresponds to a very thin trailing edge in which only one per cent of the wing mass or area is invested in the rear fourth of the wing. In figure 6, we plot τ for μ along all eight eigenmorphs. The optimal solution of $\mu = 0$ has high $\tau \approx 40$, but more striking is that the four stiffest eigenmorphs

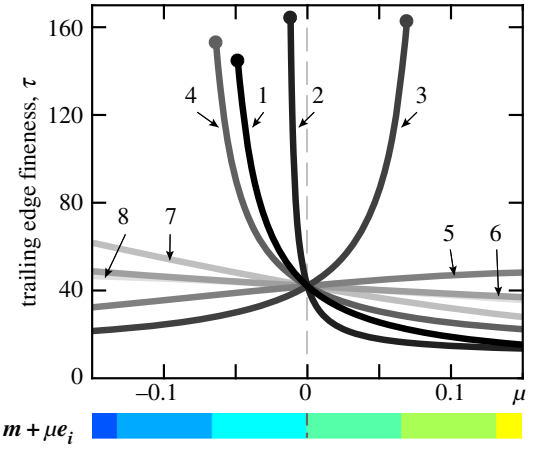

Figure 6. Evolution of the trailing edge fineness when scanning the shape space around the mean genome $\boldsymbol{m}$ along each eigenmorph $\boldsymbol{e_i}$. The fineness τ is defined as the ratio of the total cross-sectional area of the wing S to the area located within the last fourth of its chord. The four stiffest eigenmorphs are all near a rapid increase in the fineness associated with unphysical shape solutions, which occur where the displayed curves terminate.

are all quite close to an unphysical boundary (solid dots) and the associated rapid increase in τ. This suggests that the evolutionary scheme not only tends towards a thin trailing edge but is ultimately limited by the unphysical nature of a truly cusp-like structure. This is consistent with our inability to three-dimensionally print some of the later-generation candidate wings due to their exceedingly thin trailing edges.

6. Favourable traits, their emergence and structure of the optima

The eigenmorphs provide a practical and concrete characterization of the morphological changes that significantly impact performance. They may also be interpreted in terms of more intuitive geometrical parameters discussed above, such as fore-aft asymmetry as specified by the edge sharp- or blunt-ness, fineness of the trailing edge, and location of maximum thickness along the chord. Some such characterizations, such as the slenderness as measured by thickness-to-chord ratio, are commonplace in describing aero- or hydro-dynamic performance. We hypothesize that each such feature identified by the stiffest eigenmorphs in the elite population will be associated with a peak or maximum in speed when displayed for the larger population.

To test this, we define metrics for these characteristics and display in figure 7 how these relate to speed for all wings across all generations. For example, in figure 7*a* we report on the performance of wings with regard to the asymmetry in edge bluntness. In this case, the asymmetry parameter corresponds exactly to the value of the gene α_0 which governs which edge is more blunt, as explained in the Material and Methods section. Values near 0 indicate a blunt trailing edge and sharp leading edge, and *vice versa* for values near 1. While early generations display a wide range of values, wings of later generations preferentially have a blunt nose and sharp trailing end. In this case, an apparent maximum in speed occurs near one extreme in the shape parameter.

More commonly, a favourable attribute is not directly encoded by a single gene parameter. The optimum also typically occurs at an intermediate value in the parameter range. For example, in figure 7*b*, we report on how speed relates to the position of the point of maximum thickness along the wing chord. This feature, which is dictated by many genes, displays a sharp maximum near 0.2. Thus, the best wings are tightly constrained to have a thickest portion located downstream from the nose by about 20% of the chord length. As another important feature, wing slenderness

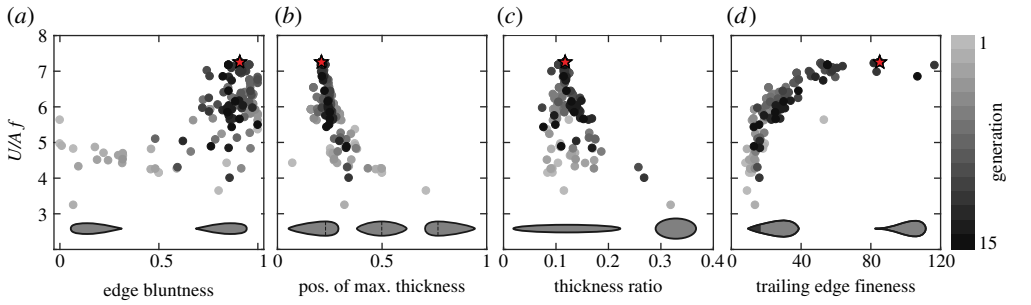

Figure 7. Evolution of attributes that correlate with locomotion speed. (*a*) Asymmetry in the bluntness of wing edges: The fastest wings have a rounded leading edge and sharp trailing edge. (*b*) Relative position along the chord of the maximum thickness. (*c*) Thickness-to-chord ratio. (*d*) Trailing edge fineness. For all plots, each wing corresponds to a point and grey scale indicates generation, with the best wing indicated by a red star. Data are shown for $A = 3$ cm and $f = 1.8$ Hz, and the trends are representative of other values of f. (Online version in colour.)

can be quantified by the ratio of thickness to chord length, which also depends on many genes and also displays a non-trivial optimum, as shown in figure 7*c*. Short and stout wings have large t/c and are universally slow, and performance improves for more slender wings. The data of figure 7*c* show an apparent peak near $0.12 \approx 1/8$, which corresponds to shapes that are about eight times longer in chord than in thickness. One also sees that, while some specific traits are shared by the very fastest wings, having any one such trait does not guarantee fast locomotion. For example, the best wings have thickness-to-chord ratio near 0.12 but other wings of this same or similar t/c move at half the maximum speed and are among the slowest of all shapes explored. Thus, optimality stems from a suite of features in combination.

The trailing edge fineness τ, as defined above, displays yet another structure as to optimality. From the data of figure 7*d*, we see that speed improves somewhat monotonically with fineness with the fastest wings having the vast majority of their mass invested in the leading portion of the chord. We suggest that the best-found solution tends to large but finite τ because of the practical limitation of manufacturing a foil of such extreme fineness.

7. Parametric analysis

The above results suggest that the teardrop form of the very fastest wing is at or near a local optimum in speed with regard to changes in shape. To corroborate this, we systematically morph this fastest profile to explore similar shapes around this suspected optimum and assess their relative performance. For example, to explore changes in the location of maximum thickness, we generate a new family of wings by applying a triangular shear transformation to the teardrop profile. This operation shifts the thickest portion along the wing chord while leaving the two edges largely unaffected. Two such foils are shown in figure 8*a*, with the thickest portion shifted towards the leading edge and towards the trailing edge, respectively. The resulting speed normalized by that of the original teardrop profile for members of this family is plotted in figure 8*a*, revealing a distinct maximum near that discovered by evolution (red star). We note that such morphing transformations in general yield shapes outside the parametrization employed in our evolutionary scheme, and thus the appearance of a peak in this dataset offers additional support for local optimality.

A similar procedure is used to explore the effect of wing slenderness. Here, we generate of family of wings of differing thickness-to-chord ratio, t/c, by applying compression or expansion transformations that preserve cross-sectional area. The measured speed data reported in figure 8*b* show that increasing slenderness, which corresponds to decreasing t/c, leads to increasing speed up until a critical $t/c \backsim 0.12$, and thereafter changes are more modest. The fastest profile (red star)

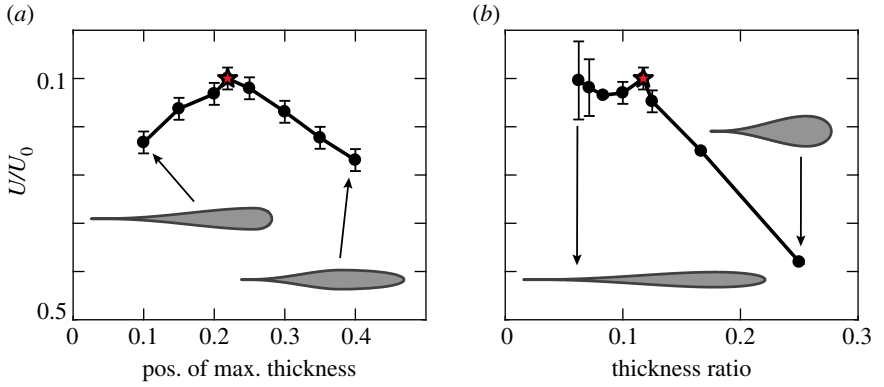

Figure 8. Exploring the speed dependence of shape attributes through systematic morphing of the fastest wing solution. The measured speed U, normalized by the maximal speed U_0 produced by evolution for wings of varying (*a*) position of maximum thickness and (*b*) thickness-to-chord ratio. The first feature displays a clear peak bounded by steep slopes, and the second shows a peak bounded by a plateau and steep slope. Data are shown $f = 1.8$ Hz. (Online version in colour.)

discovered by the evolution scheme again appears to correspond to a local peak, albeit one that is highly asymmetric and bounded between a plateau and a steep cliff. We note that the very thin profiles for small t/c are prone to slightly flex and reorient under the fluid loading, which induces larger errors in U depending on how securely the wing is mounted on its support rod.

8. Discussion and conclusion

This work demonstrates a scheme that modifies the cross-sectional shape and iteratively improves the speed of wings or hydrofoils in forward heaving-and-plunging flight. The use of an evolutionary algorithm, automated data collection, and three-dimensional printing permits the rapid exploration of many wing forms and arrival at the fastest profile after testing about 100 foils. We also present a statistical analysis that uses the population of elite foils to infer which aspects of the shape are most critical to performance. This method uses principal component analysis (PCA) to identify a natural basis of shape deformations that we call 'eigenmorphs', some which strongly degrade performance and others which induce little effect. Together, these results reveal a fastest foil that resembles an elongated teardrop with quantifiable features such as a pronounced fore-aft asymmetry in edge sharpness—including a rounded bulb at the leading edge and thinly cusped trailing edge—and a slenderness or thickness-to-chord ratio of about 0.12. Elite wings all share this suite of favourable traits, but each particular trait is also found on inferior wings, and so no single feature guarantees good performance. Though true optimality is not guaranteed by the algorithm, the results of our evolutionary and parametric studies suggest that this teardrop form is near a local maximum for speed. Our study also gives insight into the underlying fitness landscape, which exhibits clear peaks in some directions of shape space but can also show plateau-like directions where speed depends little on shape variations.

The optimal form and the most favourable features discovered here must reflect unsteady flow–shape interactions, but our study leaves unidentified the underlying fluid-dynamical mechanisms. Indeed, the evolutionary algorithm, exploration of a broad family of shapes, and eigenmorph analysis employed here are 'blind' schemes that are not biased by aero- or hydro-dynamic expectations but also do not provide physical explanations. We may speculate nonetheless as to why the elite foils perform well. The bulb-like nose provides a broader frontal region for suction pressure to act upon, which is known to be a significant source of thrust for heaving-wing flight [9,10]. Leading-edge suction may also explain why a uniformly thin, plate-like shape is not among the elite despite its drag-minimizing profile. Our results are consistent

with previous computational studies showing the existence of a thickness optimum [37], with a rounded leading edge favouring suction but overly thick profiles resulting in high drag. The location of maximum thickness, which was found for the fastest wings to be about 20% of the chord from the leading edge, may also relate to this suction, for example, by confining the low-pressure leading-edge vortex to the front of the wing. The sharply cusped trailing edge may generate strong vorticity that contributes to the propulsive jet generated by the foil [16,40,57]. The associated concavity of shape on the latter portion of the wing may also play a role in the effective imparting of momentum to the fluid [58]. Slenderness seems more subtle in light of the fact that increasing slenderness, or decreasing the thickness-to-chord ratio t/c, leads to rapidly increasing speed until a critical $t/c \sim 0.12$ and thereafter changes little. While unexplained, this observation is consistent with previous numerical simulations [34].

Because the problem considered here shares some broad features with animal flight, it is natural to compare the teardrop form to the shapes of bird wings. Avian wings tend to share the features of low thickness-to-chord ratio, a rounded and thickened leading edge, and a sharp trailing edge. While many of these are quite generic streamlined traits that are common in fixed-wing aerofoils as well, perhaps the most unique features shared by the teardrop foil and bird wings are that of an exceedingly thin downstream region that yields a cusp-like trailing edge. The trailing region of a bird wing typically thins to a remex or single feather [59], suggesting a selection towards fineness that has reached material limitations. This is reminiscent of our laboratory evolution scheme yielding solutions so thin that they test our manufacturing capabilities.

Animal flight and engineering applications that use oscillating propulsors, however, involve many additional effects not considered here, such as complex flapping kinematics and wing flexibility. Extensions of this study could seek optimal cross-sectional shape for flight that includes one or more of these factors, and these factors could also be optimized or improved along with shape. Perhaps the simplest extension would be to consider variations in amplitude while maintaining sinusoidal vertical motions. This may lead to different regimes for the amplitude-to-chord ratio, which has been shown to be an important parameter in forward flight [17,19]. A next step might be to consider variations in stroke form for heaving-and-plunging motions, and while the stroke form itself has been optimized for a fixed rectangular cross section [27], it is not clear how the shape and stroke form might influence one another. Yet another complexity would allow for the combined vertical heaving motion and pitching rotations that typify biological flapping flight. Because the angle of attack is strongly modified by pitching, the local flow may change significantly [60], an effect that could strongly alter the optimal shape. An additional layer would include wing flexibility. Previous works have shown that thrust-producing wings exhibit optimal performance for particular values of (homogeneous) stiffness [29–31]. Understanding the coupled problem of profile shape and flexibility, both of which affect the bending rigidity and deformation modes, represents a fascinating avenue for future study. Finally, allowing for span-wise variations in shape would seem to allow for new mechanisms involving three-dimensional flow structures.

In all such optimization studies, different objectives may also be considered, for example, improving locomotion efficiency or lift generated rather than the fitness function of locomotion speed. Indeed, different genetic or evolutionary algorithms could also be explored and compared to the method employed here [50,61]. Future studies may also consider numerical methods, such as computational fluid dynamics simulations, as an alternative to the experimental approach reported here. Real-time experiments can be faster than simulations for high Reynolds number conditions involving highly unsteady flows and sharp geometries, which necessitate fine time and space resolution. Our approach is largely automated via three-dimensional printing of the shapes and electronic acquisition of the speed data, so minimal human time must be invested in loading and loading the wings. In practice, we are limited to testing one generation per day by the roughly 6 h print time, which is most conveniently done overnight. Unlike most computational approaches, we expect this run time to remain largely unchanged even as the many complexities given above are considered, provided the experimental procedures can be automated.

This work shows that mimicking natural selection or evolution in controlled laboratory experiments can be an efficient means of identifying favourable solutions for unsteady

locomotion and thus might be usefully applied to the many extensions given above. We would also argue that such schemes are especially suited for understanding complex flow–structure interaction problems generally. The intrinsic challenges are well illustrated by the simplified context of heaving propulsion studied here. While one is tempted to assert that fluid-dynamical mechanisms such as leading-edge suction and vortex generation and shedding dictate the forward speed of a heaving wing, the wing motion itself also affects these mechanisms and the unsteady flow field generally. Locomotion is thus an emergent property that comes about from the flow–foil interaction, and the interaction is influenced by shape. Such complex coupling is a hallmark of a broader class of moving boundary problems and fluid–structure interactions, and evolutionary algorithms seem especially well suited for identifying desired solutions.

9. Material and methods

(a) Shape parametrization

We consider up-down symmetric wing profiles with an upper half curve described by:

$$y(x)/c = \sum_i \beta_i \left[\alpha_i \left(\frac{x}{c}\right)^i + (1-\alpha_i)\left(1-\frac{x}{c}\right)^i \right],$$

where $i = 1/2, 1, 2, 3, 4$ and $\{\beta_i, \alpha_i\}$ are coefficients specific to each profile, and c is the wing chord length. This is a modification of the four-digit NACA up-down symmetric family of foils, which employ a fourth-order polynomial and a square-root term that forms a blunt leading edge. Specifically, a NACA profile is of the form $y(x)/c = \sum_i \beta_i (x/c)^i$, which may be recovered from our formula by setting $\alpha_i = 1$. Our inclusion of the $(1 - x/c)^i$ terms allows for fore-aft symmetric or asymmetric shapes, where the parameters α_i affect the degree of symmetry. We restrict $\beta_i \in [-1, 1]$, which discriminates against short shapes but otherwise permits many shape variations. Each wing is thus characterized by eleven parameters (5 α_i terms, 5 β_i terms, and the chord c), that are reduced to eight by two end conditions $y(0) = y(c) = 0$ as well as the imposition of fixed cross-sectional area. We use the end conditions to eliminate $\beta_4 = -\sum_{i=1/2}^{3} \beta_i$ and $\alpha_4 = -\sum_{i=1/2}^{3} \alpha_i \beta_i / \beta_4$. The cross-sectional area is given by $S = 2\int_0^c y(x)\mathrm{d}x = 2c^2 \int_0^1 \sum_i \beta_i [\alpha_i u^i + (1-\alpha_i)(1-u)^i]\mathrm{d}u$, where the second form comes about by introducing $u = x/c$. We use this relationship to eliminate c. This leaves eight parameters corresponding to $\{g_i\} = \{\beta_{1/2}, \beta_1, \beta_2, \beta_3, \alpha_{1/2}, \alpha_1, \alpha_2, \alpha_3\}$, which are called 'genes' throughout the text.

(b) Experimental methods

A MakerBot Replicator 2 3D-Printer constructs wings of span length 15 cm and cross-sectional area $S = 3.5\,\mathrm{cm}^2$ out of PLA plastic with a resolution of 0.2 mm. Wings are then mounted on a radial arm that constrains swimming along a circle in the horizontal plane of radius $R = 25$ cm (measured at midspan) around a central driving shaft. A damper is attached on that same arm opposite to the wing. We apply a sinusoidal flapping motion of peak-to-peak amplitude $A = 3$ cm and vary the frequency $f \in [0.4 - 2.4]$ Hz. For each of the 150 wing shapes, swimming speed is evaluated over 11 different frequencies. Those measurements are reported in figure 9 for wings of a representative early generation as well as one of the latest, showing that U increases quasi-linearly with f and that the ordering of individuals remains the same across the frequency range, with the fastest ones performing consistently better. For the sake of clarity, we only plot measurements performed at $f = 1.8$ Hz throughout the paper, and the full dataset is available as the electronic supplementary material.

Potential interaction of the foil with the flows generated in its previous orbit is minimized by (1) slowing the swimming with the draggy damper and (2) ensuring a long circumferential travel distance around the tank. Specifically, previous experiments [21,23] on multiple wings in similar set-ups have shown that wake interactions are appreciable only for wings spaced within

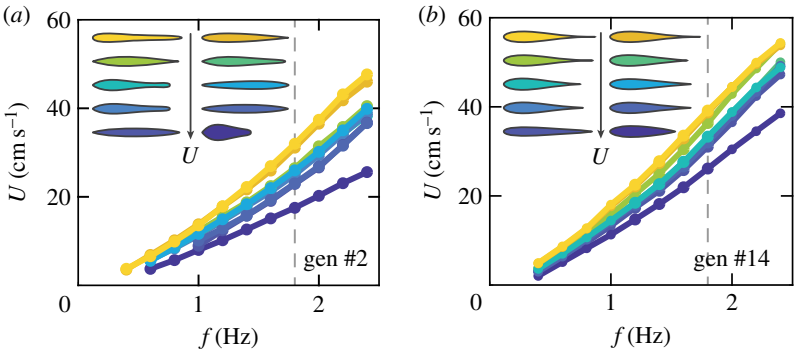

Figure 9. Speed dependence on flapping frequency. (*a*) Speed measured for flapping frequencies $f = 0.4 - 2.4$ Hz for wings of an early generation (generation 2) and (*b*) a later one (generation 14). The speed-ranking among wings, denoted by a yellow to blue colour gradient, remains the same in the frequency range tested.

about four wavelengths of motion, where the trajectory wavelength is $\lambda = U/f$. For the single-wing experiments reported here, the relevant separation distance is the circumferential length $C = 2\pi R$ of the circular trajectory, and our data indicate that $C/\lambda > 7$ for all trials. Thus, wing-wake interaction effects associated with the rotational set-up are expected to be minimal.

Any potential effect on the foil from the wake of the damper is minimized by (1) using a porous disc so as to avoid the formation of coherent vortices in its wake, and (2) affixing this damper at a shorter radius from the central axle such that it does not overrun the same path as the wing. Specifically, the damper is a disc of diameter 7 cm with porosity of about 1/3, for which previous measurements indicate a drag coefficient of about 1.0 [62]. The damper is located 10 cm outwards from the central shaft, significantly less than the 25 cm radial length to the mid-span of the wings. To test for any damper–foil interactions, we compare the speed of a typical wing for conditions in which the damper is placed 90° ahead of the wing, opposite the wing at 180°, and 90° behind the wing. No discernable difference in speed was measured, which we take as evidence for minimal interference.

(c) Evolutionary algorithm

The fitness is defined such as to account for the speeds across all measured frequencies f. For each wing and each f in each generation, the speed U is experimentally measured, and $U(f)$ curves for all individuals in two representative generations are shown in figure 9. Although U tends to increase with f for all wings, it is seen that the relative speed-ranking of different wings tends to remain unchanged across different f. This motivates a fitness metric defined at each f and for each individual of speed U: $(U - U_{\min})/(U_{\max} - U_{\min}) \in [0, 1]$, where $U_{\min}$ is lowest speed across all individuals of the generation at each f, and $U_{\max}$ is the highest. This linearly maps the speed data such that the slowest wing is assigned fitness 0 and the fastest is given fitness of 1. The overall fitness $F \in [0, 1]$ of each wing is then defined to be the average of these quantities across all f. This metric is a robust characterization of relative performance within a generation that employs speed data collected at all values of f and weights all such data equally.

Following the evaluation of the fitness of the wings, each new generation of ten wings is then created from the previous one using a custom Matlab algorithm adapted from [54]. First, two parents are selected from the entire population of ten wings through fitness proportionate selection. That is, the selection of each is made independently and with a probability determined by each wing's fitness: $P_i = F_i / \sum_j F_j$, where the sum is computed over all ten members of a generation. After two parents are identified, breeding involves the recombination of their genomes $\boldsymbol{p_1}$ and $\boldsymbol{p_2}$ into a daughter shape $\boldsymbol{d}$ through a weighted average: $\boldsymbol{d} = r\ \boldsymbol{p_1} + (1 - r)\boldsymbol{p_2}$,

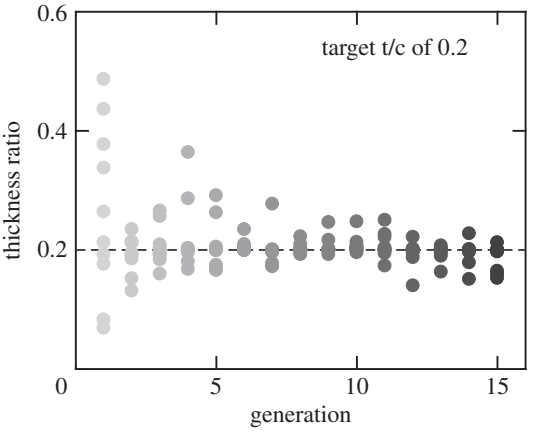

Figure 10. Evolutionary algorithm tested to reach a targeted thickness ratio. Representative run, showing the evolution of the thickness ratio of wings over successive generations with convergence towards the target $t/c = 0.2$ within about 10 iterations.

where $r \in [0, 1]$ is a random number. The daughter wing is also subject to mutations, which occur with a probability of 20% and act to randomly modify a gene value. The applied perturbation follows a normal distribution with a standard deviation of one-fourth of the gene value. This process of selecting two parents for breeding by gene combination and mutation to form a daughter is repeated to yield eight daughters of the next generation. Parents may be selected multiple times and thus seed multiple daughters, and indeed a parent may breed with itself. In addition, the two fastest wings of the current generation are transferred unmodified to the next, yielding a new population totalling 10 wings. This passing-through of the two fittest individuals ensures that the maximum fitness does not decrease from generation to generation.

To tune the implementation parameters in this algorithm, prior to the study we tested the number of iterations required to meet a criterion that can be evaluated *in silico*, such as a targeted thickness ratio. Figure 10 shows an evolution run aimed at producing wings with thickness ratio $t/c = 0.2$, where the fitness of an individual is defined as the inverse of the deviation of its t/c from the targeted value. The algorithm typically reaches its objective within about 10 generations. We also opted for a high mutation rate that ensures high variability in the population. Although an in-depth tuning of the algorithm remains for future studies, the chosen parameters thus allow for a broad exploration of the high-dimensional shape space within experimentally tractable timescales.

Data accessibility. The dataset supporting this article, along with a movie of the experimental apparatus, have been uploaded as part of the electronic supplementary material.

Authors' contributions. S.R. and L.R. conceived and designed research; S.R. and T.M. performed research and data acquisition; S.R., T.M. and L.R. analysed and interpreted data; S.R. and L.R. wrote the paper. All authors gave final approval for publication.

Competing interests. The authors declare no competing interests.

Funding. We acknowledge support from an NYU Global Seed grant to L.R. and from the Direction Générale de l'Armement (2013.60.0018) to S.R.

Acknowledgements. We thank S. Childress, M. Shelley and J. Zhang for discussions.

References

1. Anderson Jr JD. 1997 *A history of aerodynamics: and its impact on flying machines*, vol. 8. Cambridge, UK: Cambridge University Press.
2. Anderson Jr JD. 1984 *Fundamentals of aerodynamics*. New York, NY: McGraw-Hill.
3. Wu TY. 2011 Fish swimming and bird/insect flight. *Annu. Rev. Fluid Mech.* **43**, 25–58. (doi:10.1146/annurev-fluid-122109-160648)

4. Rozhdestvensky KV, Ryzhov VA. 2003 Aerohydrodynamics of flapping-wing propulsors. *Prog. Aerosp. Sci.* **39**, 585–633. (doi:10.1016/S0376-0421(03)00077-0)
5. Paranjape AA, Dorothy MR, Chung SJ, Lee KD. 2012 A flight mechanics-centric review of bird-scale flapping flight. *Int. J. Aeronaut. Space Sci.* **13**, 267–281. (doi:10.5139/IJASS.2012.13.3.267)
6. Knoller R. 1909 Die Gesetze des Luftwiderstandes. *Flug-und Motortechnik (Wien)* **3**, 1–7.
7. Betz A. 1912 Ein beitrag zur erklaerung des segelfluges. *Z. für Flugtechnik und Motorluftschiffahrt* **3**, 269–272.
8. Katzmayr R. 1922 Effect of periodic changes of angle of attack on behavior of airfoils. NACA TR TM 147.
9. Garrick IE. 1937 Propulsion of a flapping and oscillating airfoil. NACA Report No. 567.
10. Wu TYT. 1961 Swimming of a waving plate. *J. Fluid Mech.* **10**, 321–344. (doi:10.1017/S0022112061000949)
11. Lighthill MJ. 1970 Aquatic animal propulsion of high hydromechanical efficiency. *J. Fluid Mech.* **44**, 265–301. (doi:10.1017/S0022112070001830)
12. von Kármán T, Burgers J. 1935 *General aerodynamic theory - perfect fluids*. Aerodynamic Theory, vol. 2. Berlin, Germany: Springer.
13. Vandenberghe N, Zhang J, Childress S. 2004 Symmetry breaking leads to forward flapping flight. *J. Fluid Mech.* **506**, 147–155. (doi:10.1017/S0022112004008468)
14. Alben S, Shelley M. 2005 Coherent locomotion as an attracting state for a free flapping body. *Proc. Natl Acad. Sci. USA* **102**, 11 163–11 166. (doi:10.1073/pnas.0505064102)
15. Triantafyllou MS, Triantafyllou GS, Yue DKP. 2000 Hydrodynamics of fishlike swimming. *Annu. Rev. Fluid Mech.* **32**, 33–53. (doi:10.1146/annurev.fluid.32.1.33)
16. Godoy-Diana R, Aider JL, Wesfreid JE. 2008 Transitions in the wake of a flapping foil. *Phys. Rev. E* **77**, 016308. (doi:10.1103/PhysRevE.77.016308)
17. Anderson JM, Streitlien K, Barrett DS, Triantafyllou MS. 1998 Oscillating foils of high propulsive efficiency. *J. Fluid Mech.* **360**, 41–72. (doi:10.1017/S0022112097008392)
18. Wang ZJ. 2000 Vortex shedding and frequency selection in flapping flight. *J. Fluid Mech.* **410**, 323–341. (doi:10.1017/S0022112099008071)
19. Lewin GC, Haj-Hariri H. 2003 Modelling thrust generation of a two-dimensional heaving airfoil in a viscous flow. *J. Fluid Mech.* **492**, 339–362. (doi:10.1017/S0022112003005743)
20. Platzer MF, Jones KD, Young J, Lai JCS. 2008 Flapping wing aerodynamics: progress and challenges. *AIAA J.* **46**, 2136–2149. (doi:10.2514/1.29263)
21. Becker AD, Masoud H, Newbolt JW, Shelley M, Ristroph L. 2015 Hydrodynamic schooling of flapping swimmers. *Nat. Commun.* **6**, 8514. (doi:10.1038/ncomms9514)
22. Agre N, Childress S, Zhang J, Ristroph L. 2016 Linear drag law for high-Reynolds-number flow past an oscillating body. *Phys. Rev. Fluids* **1**, 033202. (doi:10.1103/PhysRevFluids.1.033202)
23. Ramananarivo S, Fang F, Oza A, Zhang J, Ristroph L. 2016 Flow interactions lead to orderly formations of flapping wings in forward flight. *Phys. Rev. Fluids* **1**, 071201. (doi:10.1103/PhysRevFluids.1.071201)
24. Read DA, Hover FS, Triantafyllou MS. 2003 Forces on oscillating foils for propulsion and maneuvering. *J. Fluids Struct.* **17**, 163–183. (doi:10.1016/S0889-9746(02)00115-9)
25. Hover FS, Haugsdal Ø, Triantafyllou MS. 2004 Effect of angle of attack profiles in flapping foil propulsion. *J. Fluids Struct.* **19**, 37–47. (doi:10.1016/j.jfluidstructs.2003.10.003)
26. Xiao Q, Liao W. 2010 Numerical investigation of angle of attack profile on propulsion performance of an oscillating foil. *Comput. Fluids* **39**, 1366–1380. (doi:10.1016/j.compfluid.2010.04.006)
27. Roberts JW, Moret L, Zhang J, Tedrake R. 2010 Motor learning at intermediate Reynolds number: experiments with policy gradient on the flapping flight of a rigid wing. In *From motor learning to interaction learning in robots*, pp. 293–309. Berlin, Germany: Springer.
28. Shyy W, Aono H, Chimakurthi SK, Trizila P, Kang CK, Cesnik CES, Liu H. 2010 Recent progress in flapping wing aerodynamics and aeroelasticity. *Prog. Aerosp. Sci.* **46**, 284–327. (doi:10.1016/j.paerosci.2010.01.001)
29. Masoud H, Alexeev A. 2010 Resonance of flexible flapping wings at low Reynolds number. *Phys. Rev. E* **81**, 056304. (doi:10.1103/PhysRevE.81.056304)
30. Ramananarivo S, Godoy-Diana R, Thiria B. 2011 Rather than resonance, flapping wing flyers may play on aerodynamics to improve performance. *Proc. Natl Acad. Sci. USA* **108**, 5964–5969. (doi:10.1073/pnas.1017910108)

31. Quinn DB, Lauder GV, Smits AJ. 2014 Scaling the propulsive performance of heaving flexible panels. *J. Fluid Mech.* **738**, 250–267. (doi:10.1017/jfm.2013.597)
32. Lentink D, Gerritsma M. 2003 Influence of airfoil shape on performance in insect flight. In *33rd AIAA Fluid Dynamics Conference and Exhibit, Orlando, FL, 23–26 June*. p. 3447. AIAA.
33. Vandenberghe N, Childress S, Zhang J. 2006 On unidirectional flight of a free flapping wing. *Phys. Fluids* **18**, 014102. (doi:10.1063/1.2148989)
34. Zhang X, Ni S, Wang S, He G. 2009 Effects of geometric shape on the hydrodynamics of a self-propelled flapping foil. *Phys. Fluids* **21**, 103302. (doi:10.1063/1.3251045)
35. An S, Maeng J, Han C. 2009 Thickness effect on the thrust generation of heaving elliptic airfoils. *J. Aircraft* **46**, 216–222. (doi:10.2514/1.37903)
36. Zhao L, Yang S. 2010 Influence of thickness variation on the flapping performance of symmetric NACA airfoils in plunging motion. *Math. Probl. Eng.* **2010**, Article ID 675462. (doi:10.1155/2010/675462)
37. Ashraf MA, Young J, Lai JCS. 2011 Reynolds number, thickness and camber effects on flapping airfoil propulsion. *J. Fluids Struct.* **27**, 145–160. (doi:10.1016/j.jfluidstructs.2010.11.010)
38. La Mantia M, Dabnichki P. 2011 Effect of the wing shape on the thrust of flapping wing. *Appl. Math. Model.* **35**, 4979–4990. (doi:10.1016/j.apm.2011.04.003)
39. Yu M, Wang ZJ, Hu H. 2012 Airfoil thickness effects on the thrust generation of plunging airfoils. *J. Aircraft* **49**, 1434–1439. (doi:10.2514/1.C031720)
40. 2008 Computational study of unsteady low-Reynolds-number airfoil aerodynamics using moving overlapping meshes. *AIAA J.* **46**, 429–438. (doi:10.2514/1.31499)
41. Cebeci T, Platzer M, Chen H, Chang KC, Shao JP. 2005 *Analysis of low-speed unsteady airfoil flows*. Berlin, Heidelberg: Springer.
42. Michalewicz Z. 1996 *Genetic algorithms+ data structures= evolution programs*. Berlin, Germany: Springer Science & Business Media.
43. Davis L. 1991 *Handbook of genetic algorithms*, vol. 115. New York, NY: Van Nostrand Reinhold.
44. Back T. 1996 *Evolutionary algorithms in theory and practice: evolution strategies, evolutionary programming, genetic algorithms*. Oxford, UK: Oxford University Press.
45. Bentley P. 1999 *Evolutionary design by computers*. Los Altos, CA: Morgan Kaufmann.
46. Lipson H, Pollack JB. 2000 Automatic design and manufacture of robotic lifeforms. *Nature* **406**, 974–978. (doi:10.1038/35023115)
47. Hunt R, Hornby GS, Lohn JD. 2005 Toward evolved flight. In *Proc. of the 7th Annual Conf. on Genetic and Evolutionary Computation, Washington, DC, 25–29 June*, pp. 957–964. New York, NY: ACM.
48. Eloy C. 2013 On the best design for undulatory swimming. *J. Fluid Mech.* **717**, 48–89. (doi:10.1017/jfm.2012.561)
49. Olhofer M, Yankulova D, Sendhoff B. 2011 Autonomous experimental design optimization of a flapping wing. *Genet. Program. Evol. Mach.* **12**, 23–47. (doi:10.1007/s10710-010-9107-0)
50. van Rees WM, Gazzola M, Koumoutsakos P. 2015 Optimal morphokinematics for undulatory swimmers at intermediate Reynolds numbers. *J. Fluid Mech.* **775**, 178–188. (doi:10.1017/jfm.2015.283)
51. Miskin MZ, Jaeger HM. 2013 Adapting granular materials through artificial evolution. *Nat. Mater.* **12**, 326–331. (doi:10.1038/nmat3543)
52. Milano M, Gharib M. 2005 Uncovering the physics of flapping flat plates with artificial evolution. *J. Fluid Mech.* **534**, 403–409. (doi:10.1017/S0022112005004842)
53. Wolff K, Sandberg D, Wahde M. 2008 Evolutionary optimization of a bipedal gait in a physical robot. In *Evolutionary Computation, 2008. CEC 2008. (IEEE World Congress on Computational Intelligence)*, pp. 440–445. Piscataway, NJ: IEEE.
54. Spall JC. 2005 *Introduction to stochastic search and optimization: estimation, simulation, and control*, vol. 65. New York, NY: John Wiley & Sons.
55. Hornby GS, Takamura S, Yamamoto T, Fujita M. 2005 Autonomous evolution of dynamic gaits with two quadruped robots. *IEEE Trans. Robot.* **21**, 402–410. (doi:10.1109/TRO.2004.839222)
56. Taylor GK, Nudds RL, Thomas ALR. 2003 Flying and swimming animals cruise at a Strouhal number tuned for high power efficiency. *Nature* **425**, 707–711. (doi:10.1038/nature02000)
57. Lai SJoseph C, Platzer MF. 2001 Characteristics of a plunging airfoil at zero freestream velocity. *AIAA J.* **39**, 531–534. (doi:10.2514/3.14764)
58. van Rees WM, Gazzola M, Koumoutsakos P. 2013 Optimal shapes for anguilliform swimmers at intermediate Reynolds numbers. *J. Fluid Mech.* **722**, R3. (doi:10.1017/jfm.2013.157)

59. Dhawan S. 1991 Bird flight. *Sadhana* **16**, 275–352. (doi:10.1007/BF02745345)
60. Isogai K, Shinmoto Y, Watanabe Y. 1999 Effects of dynamic stall on propulsive efficiency and thrust of flapping airfoil. *AIAA J.* **37**, 1145–1151. (doi:10.2514/2.589)
61. Olhofer M, Jin Y, Sendhoff B. 2001 Adaptive encoding for aerodynamic shape optimization using evolution strategies. In *Proc. of the 2001 Congress on Evolutionary Computation, Seoul, Korea, 27–30 May*, vol. 1, pp. 576–583. Piscataway, NJ: IEEE.
62. Theunissen R, Worboys R. 2018 Near-wake observations behind azimuthally perforated disks with varying hole layout and porosity in smooth airstreams at high Reynolds numbers. *J. Fluids Eng.* **141**, 051108. (doi:10.1115/1.4041614)